Mixed Third Harmonic Shear Horizontal Wave Generation: Interaction between Primary Shear Horizontal Wave and Second Harmonic Lamb Wave

Shengbo Shan and Li Cheng*

Department of mechanical engineering, The Hong Kong Polytechnic University, Kowloon, Hong Kong.

E-mail: li.cheng@polyu.edu.hk

Abstract

The third harmonic shear horizontal (SH) waves in a weakly nonlinear plate provide new possibilities for incipient damage detections. The understanding of their generation mechanism, however, is limited to the intuitive process of cubic self-interaction of the primary SH waves. By considering both the third order and fourth order elastic constants (TOECs and FOECs), this paper reports the discovery of a new generation mechanism, referred to as mixed generation, which results from the mutual interaction between the primary SH waves and their induced second harmonic Lamb waves. Compared with linearly cumulative third harmonic SH waves induced by the cubic self-interaction of the primary SH waves, the mixed third harmonic SH wave amplitude also increases with the wave propagating distance but in a wavering manner according to the phase velocity matching condition. Upon establishing a complex-domain superposition method

which allows a precise extraction of the third harmonic responses, the significance and the propagating characteristics of the mixed third harmonic SH waves are numerically investigated through finite element simulations. Experiments are then conducted with a dedicated subtraction scheme to highlight the material nonlinearity of interest. A gel test is designed and carried out to identify the two types of third harmonic SH wave components from the measured time-domain signals. Both numerical and experimental results confirm the existence and the significance of the mixed third harmonic SH generation mechanism, which may impact on further applications, especially underwater damage inspections.

Key words: mixed third harmonic SH waves, cumulative effect, complex-domain superposition method, subtraction scheme

Introduction

Higher-order harmonic ultrasonic guided waves, usually resulting from the microstructural defects in a waveguide, provide a promising and feasible means for incipient damage detections [1, 2]. Most existing efforts focus on the second harmonic Lamb waves (2^{nd} Lamb waves) in weakly nonlinear plates in both theoretical and applied perspectives [3-10]. Theoretical studies prove that the 2^{nd} Lamb waves can be generated if only the power flux from the primary mode to the second harmonic mode is nonzero [5, 6]. This suggests that, whatever the primary wave mode is (symmetric or antisymmetric Lamb waves or symmetric or antisymmetric SH waves), the second harmonic wave filed should only be the symmetric Lamb waves [3, 6]. Furthermore, if the phase

velocities of the primary and second wave modes (approximately) match, the generated second harmonic Lamb waves are cumulative with respect to the propagating distance, which can be further explored for damage detection applications [5, 6, 11]. Restricted by these two conditions, however, only a limited number of frequency-dependent mode pairs can be used for damage detection applications [6, 11]. Based on these predetermined mode pairs, the second harmonic Lamb waves have been applied for the detection of various types of structural or material detect such as fatigue [8], thermal aged damage [9], plastic deformation [7] and so forth.

Recently, Liu *et al.* studied the generation and propagation characteristics of the third harmonic SH waves (3rd SH waves), pointing at new possibilities for damage detection applications [12-14]. In contrast to the 2nd Lamb waves, the 3rd SH waves are shown to be holo-internal-resonant with the primary SH waves (1st SH waves) at all frequencies so that their amplitudes will always be cumulative [12]. This frequency-independent feature offers tremendous flexibility for the choice of the excitation frequency for damage detection applications. In addition, it was experimentally demonstrated that the 3rd SH waves are more sensitive to incipient plastic damage than the 2nd Lamb waves are [13], which can significantly shift the damage detection limit to the earlier stage.

As compared to the 2nd Lamb waves, however, relevant research on the 3rd SH waves is still in its infancy and relatively scarce. The lack of understanding of some major issues, at both fundamental and applied levels, bottlenecks the damage detection applications of 3rd SH waves. Up to now, the generation of the 3rd SH waves has been solely attributed to the self-interaction of the 1st SH waves [12], although there are indications that the influence of the secondary wave

fields generated by the primary waves should be also considered [15]. Generally speaking, a full understanding of the underlying mechanism of the third harmonic SH wave generation is still lacking. The exploration of the topic is technically challenging, hampered by the obvious deficiencies in the existing tools, either numerical or experimental. For example, in the numerical perspective, the fourth order elastic constants (FOECs) are usually neglected which might be crucial for the 3rd SH wave generation [14, 16]. In the experimental perspective, the influence of various nonlinear components in a system may easily overwhelm the small amplitude of the 3rd SH waves induced by the material nonlinearity.

Motivated by this, this paper explores the mechanism of the 3rd SH wave generation. Through encompassing the full set of material parameters (third- and fourth-order elastic constants, TOECs and FOECs), the mechanism behind the third harmonic wave generation is systematically investigated. In addition to the well-known pure third harmonic generation, resulting from the direct cubic self-interaction of the 1st SH waves due to the FOECs for cubic material nonlinearity, a so-called mixed third harmonic SH wave generation mechanism is revealed and highlighted as the quadratic interaction between the 1st SH waves and their generated 2nd Lamb waves induced by TOECs for the quadratic material nonlinearity. Through finite element (FE) simulations, the significance and the propagating characteristics of the mixed 3rd SH waves are quantified. Specifically, a complex-domain superposition method is proposed, which allows the separation and characterization of the third harmonic responses. Then, experiments are conducted with a specially designed subtraction scheme to extract the material nonlinearity of interest. A gel test is then designed and carried out to confirm the existence as well as the influence of the mixed 3rd SH

waves. The discovered mixed third harmonic generation mechanism, through the involvement of the second harmonic Lamb wave field, should have a significant impact on further underwater applications from the wave energy leakage perspective.

Theoretical analyses

The mechanism of the third harmonic generation by the primary SH waves is first investigated from a qualitative perspective. For the sake of simplicity in the equation derivation, SH0 waves are considered. First, the material nonlinear elastic behaviors are discussed, paving the way for subsequent analyses. Then, the second harmonic generation by the 1st SH waves is briefly recalled. Finally, with the knowledge of the generated second harmonic wave field, the 3rd SH waves are studied, highlighting their generation mechanism and characteristics, with special emphasis put on the mixed 3rd SH waves.

Material nonlinear stress-strain relationship

The material nonlinear stress-strain relationship considering the fourth order expansion of the strain energy can be expressed with the extended Landau-Lifshitz model [12], as

$$\begin{aligned}\mathbf{T} = {} & \lambda tr[\mathbf{E}] + 2\mu\mathbf{E} + \overline{A}\mathbf{E}^2 + \overline{B}tr[\mathbf{E}^2]\mathbf{I} + 2\overline{B}tr[\mathbf{E}]\mathbf{E} + \overline{C}\left(tr[\mathbf{E}]\right)^2\mathbf{I} \\ & + \overline{E}tr[\mathbf{E}^3]\mathbf{I} + 3\overline{E}tr[\mathbf{E}]\mathbf{E}^2 + 2\overline{F}tr[\mathbf{E}]tr[\mathbf{E}^2]\mathbf{I} + 2\overline{F}\left(tr[\mathbf{E}]\right)^2\mathbf{E} + 4\overline{G}tr[\mathbf{E}^2]\mathbf{E} + 4\overline{H}\left(tr[\mathbf{E}]\right)^3\mathbf{I}\end{aligned} \tag{1}$$

where λ and μ are Lamé constants; $\overline{A}, \overline{B}, \overline{C}$ are the Landau TOECs while $\overline{E}, \overline{F}, \overline{G}, \overline{H}$ are the Landau FOECs of an isotropic material. The operation *tr*() denotes the trace of a matrix. In the

equation, **T** is the second Piola-Kirchhoff stress tensor and **E** the Lagrangian strain tensor. Upon omitting the geometric nonlinearity (GN), which will be further proven to be negligible in our cases, the Lagrangian strain retreats to Cauchy's strain $\boldsymbol{\varepsilon}$ and the Cauchy stress $\boldsymbol{\sigma}$ can be used instead of the second Piola-Kirchhoff stress. Details on individual components of the stress-strain relation can be found in Appendix A.

For a weakly nonlinear wave generation problem, the amplitude of the higher harmonic waves is usually much smaller than that of the primary waves. Therefore, the perturbation theory can be applied to decompose the stress into linear and nonlinear parts, as

$$\boldsymbol{\sigma} = \boldsymbol{\sigma}^{L} + \boldsymbol{\sigma}^{NL} \tag{2a}$$

$$\boldsymbol{\sigma}^{L} = \lambda tr[\boldsymbol{\varepsilon}] + 2\mu\boldsymbol{\varepsilon} \tag{2b}$$

$$\begin{aligned}\boldsymbol{\sigma}^{NL} = {} & \overline{A}\boldsymbol{\varepsilon}^2 + \overline{B}tr[\boldsymbol{\varepsilon}^2]\mathbf{I} + 2\overline{B}tr[\boldsymbol{\varepsilon}]\boldsymbol{\varepsilon} + \overline{C}\left(tr[\boldsymbol{\varepsilon}]\right)^2\mathbf{I} \\ & + \overline{E}tr[\boldsymbol{\varepsilon}^3]\mathbf{I} + 3\overline{E}tr[\boldsymbol{\varepsilon}]\boldsymbol{\varepsilon}^2 + 2\overline{F}tr[\boldsymbol{\varepsilon}]tr[\boldsymbol{\varepsilon}^2]\mathbf{I} + 2\overline{F}\left(tr[\boldsymbol{\varepsilon}]\right)^2\boldsymbol{\varepsilon} + 4\overline{G}tr[\boldsymbol{\varepsilon}^2]\boldsymbol{\varepsilon} + 4\overline{H}\left(tr[\boldsymbol{\varepsilon}]\right)^3\mathbf{I}\end{aligned} \tag{2c}$$

in which superscript *L* and *NL* denote the linear and nonlinear terms, respectively.

The second harmonic generation

Consider plane SH0 waves propagating along the *x* direction in a weakly nonlinear plate, as shown in Fig. 1. The particles of the SH0 waves move along the *z* direction. The SH0 wave field can be described in terms of the strains and only the component ε_{13}^{L} exists [17], as

$$\varepsilon_{13}^{L}=\frac{i}{2}A^{L}\overline{\varepsilon_{13}^{L}}(y)k_{SH}^{L}e^{ik_{SH}^{L}x}=\frac{i}{2}A^{L}k_{SH}^{L}e^{ik_{SH}^{L}x} \tag{3}$$

where the superscript L denotes the linear wave components. $\overline{\varepsilon_{13}^{L}}(y)$ is the normalized strain distribution across the plate thickness. For SH0 waves, the strain is uniformly distributed, as $\overline{\varepsilon_{13}^{L}}(y)=1$. A^{L} is the modal participation factor which is also called modal amplitude. k_{SH}^{L} denotes the wave number of the linear SH0 waves while x represents the wave propagating distance.

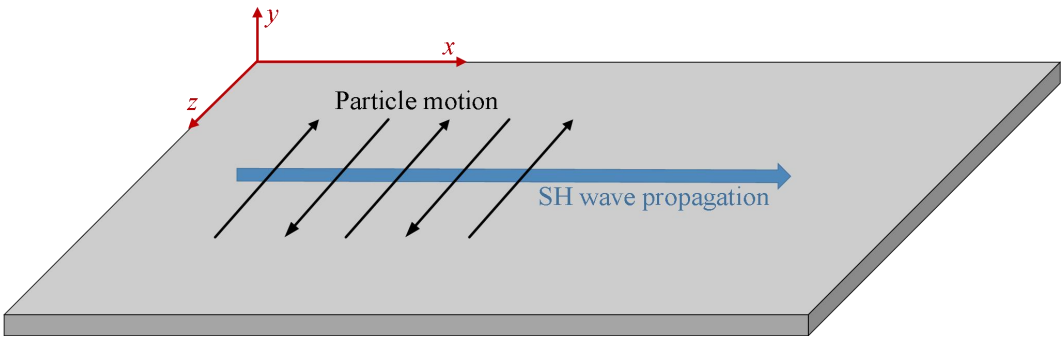

Figure 1. Sketch of the plate and the coordinate system.

When SH waves propagate in a weakly nonlinear plate, higher harmonic waves are generated. First, the second harmonic generation is considered. According to the perturbation theory, the linear wave strains of the 1st SH waves should be substituted into Eq. (2c) to calculate the nonlinear stresses which correspond to the higher harmonic generation. As only the strain component ε_{13}^{L} exists in the primary wave field, those nonlinear stress terms with an order higher than $\left(\varepsilon_{13}^{L}\right)^{2}$ can be omitted. Therefore, the remaining non-zero stress terms write

$$\sigma_{11}^{NL}=\sigma_{11}^{Q}=\overline{A}\left(\varepsilon_{13}^{L}\right)^{2}+2\overline{B}\left(\varepsilon_{13}^{L}\right)^{2} \tag{4a}$$

$$\sigma_{22}^{NL}=\sigma_{22}^{Q}=2\overline{B}\left(\varepsilon_{13}^{L}\right)^{2} \tag{4b}$$

$$\sigma_{33}^{NL} = \sigma_{33}^{Q} = \overline{A}\left(\varepsilon_{13}^{L}\right)^2 + 2\overline{B}\left(\varepsilon_{13}^{L}\right)^2 \tag{4c}$$

where the superscript Q stands for the quadratic nonlinear terms. It can be seen that only three normal nonlinear stresses exist, indicating that only the second harmonic Lamb waves can be generated, consistent with the existing theories [5, 6].

The generated nonlinear wave field can be described with the combination of the complex reciprocity relation and the normal mode expansion method with the following equations [18]:

$$4P_{nn}\left(\frac{\partial}{\partial x} - i\widetilde{\xi_n}\right)a_n(x) = \left(\widetilde{\mathbf{v}_\mathbf{n}} \cdot \boldsymbol{\sigma}^{surf} + \mathbf{v}^e \cdot \widetilde{\boldsymbol{\sigma}_\mathbf{n}}\right) \cdot \hat{\mathbf{y}}\Big|_{-d}^{d} + \int_{-d}^{d} \widetilde{\mathbf{v}_\mathbf{n}} \cdot \mathbf{F}^{vol} \mathrm{d}y \tag{5a}$$

with

$$P_{nn} = -\frac{1}{4}\int_{-d}^{d}\left[\widetilde{\mathbf{v}_\mathbf{n}(y)} \cdot \boldsymbol{\sigma}_\mathbf{n}(y) + \mathbf{v}_\mathbf{n}(y) \cdot \widetilde{\boldsymbol{\sigma}_\mathbf{n}(y)}\right] \cdot \hat{\mathbf{x}} \mathrm{d}y \tag{5b}$$

where d is the half thickness of the plate. $\mathbf{v}_\mathbf{n}(y)$ and $\boldsymbol{\sigma}_\mathbf{n}(y)$ are the velocity and stress across the thickness of the nth wave mode. The overtilde represents the complex conjugate. ξ_n is the wave number and $a_n(x)$ is the modal amplitude of a specific wave mode; $\boldsymbol{\sigma}^{surf}$, $\mathbf{v}^e$ and $\mathbf{F}^{vol}$ are the external excitations expressed as the surface traction, velocity excitation, and volume force, respectively. In this case, the excitations to generate the nonlinear waves can be obtained from the nonlinear stresses in terms of the surface traction and volume force as

$$\boldsymbol{\sigma}^{surf} = -\boldsymbol{\sigma}^{NL} \cdot \hat{\mathbf{y}} \tag{6a}$$

$$\mathbf{F}^{vol} = \nabla \cdot \boldsymbol{\sigma}^{NL} \tag{6b}$$

Substituting Eqs. (6a) and (6b) into Eq. (5a), the modal amplitude of the generated second harmonic symmetric Lamb waves can be obtained as [5, 6]

$$a_n^Q(x) = A^Q \begin{cases} \dfrac{i}{\widetilde{k_{Lamb}^Q} - 2k_{SH}^L}\left(e^{i2k_{SH}^L x} - e^{i\widetilde{k_{Lamb}^Q} x}\right) & for \quad \widetilde{k_{Lamb}^Q} \neq 2k_{SH}^L \\ xe^{i2k_{SH}^L x} & for \quad \widetilde{k_{Lamb}^Q} = 2k_{SH}^L \end{cases} \tag{7}$$

where A^Q is a coefficient related to the power flux from the primary waves to the second harmonic waves. It is worth noting that this coefficient is only related to the material nonlinearity through TOECs. This feature is crucial to further analyses.

Eq. (7) shows that if the phase velocity of the 1st SH0 wave matches with that of the 2nd Lamb waves, the generated second harmonic amplitude will be linearly cumulative. Otherwise, it will be bounded with respect to the wave propagating distance. Unfortunately, due to the dispersion characteristic of Lamb waves, very few 1st SH wave-2nd Lamb wave mode pairs can satisfy the condition of phase velocity matching [6]. Therefore, except these mode pairs at some specific frequencies, in most cases where the phase velocities of the 1st SH waves and 2nd Lamb waves do not match, the strain components of the generated 2nd Lamb waves can be generally written as

$$\varepsilon_{11}^Q = A_1^Q(\omega, y)\left(e^{i2k_{SH}^L x} - e^{i\widetilde{k_{Lamb}^Q} x}\right) \tag{8a}$$

$$\varepsilon_{22}^Q = A_2^Q(\omega, y)\left(e^{i2k_{SH}^L x} - e^{i\widetilde{k_{Lamb}^Q} x}\right) \tag{8b}$$

$$\varepsilon_{12}^Q = A_3^Q(\omega, y)\left(e^{i2k_{SH}^L x} - e^{i\widetilde{k_{Lamb}^Q} x}\right) \tag{8c}$$

where $A_1^Q(\omega, y)$, $A_2^Q(\omega, y)$ and $A_3^Q(\omega, y)$ are the generalized amplitudes which encompass the Lamb wave structure (the wave field distribution across the plate thickness). From the material perspective, these second harmonic amplitudes are only related to the TOECs. It is worth noting the strain term ε_{12}^Q is generated by the propagating second harmonic Lamb waves although the nonlinear stress term σ_{12}^Q does not exist.

The third harmonic generation

Following the same procedure, the third harmonic wave field generated by the 1st SH0 wave is investigated. First, the nonlinear stresses are calculated. For the third harmonic generation problem, all the terms in the order of $\left(\varepsilon_{13}^L\right)^3$ will be kept. Due to the existence of the second harmonic Lamb waves, their corresponding strain components ε_{11}^Q, ε_{22}^Q and ε_{12}^Q in the order of $\left(\varepsilon_{13}^L\right)^2$ should also be considered in the calculations. Based on this, the following terms corresponding to the third harmonic generation remain, as

$$\sigma_{13}^{NL} = \sigma_{13}^{C} = 2\overline{B}(\varepsilon_{11}^Q + \varepsilon_{22}^Q)\varepsilon_{13}^L + \overline{A}\left(\varepsilon_{11}^Q \varepsilon_{13}^L\right) + 8\overline{G}{\varepsilon_{13}}^3 \tag{9a}$$

$$\sigma_{23}^{NL} = \sigma_{23}^{C} = \overline{A}\varepsilon_{12}^Q \varepsilon_{13}^L \tag{9b}$$

where terms with a superscript *C* stand for the cubic nonlinear terms. The above equations show that only third harmonic shear stresses can exist, which means the third harmonic wave field generated by 1st SH waves should also be SH wave modes, which is also consistent with the existing understanding [12].

The nonlinear stress terms in Eqs. (9a) and (9b) can be classified into two categories, to be associated with two different wave generation mechanisms. The first group only involves FOECs-induced term (the third term in the right-hand-side of Eq. (9a)) where only the primary strain is involved. As the FOECs are intuitively responsible for the third harmonic generation which has been widely accepted in the open literature, the corresponding 3rd SH waves components are therefore referred to as the pure 3rd SH waves. Meanwhile, Eqs. (9a) and (9b) also show the presence of the second group of nonlinear stress terms which contains the TOECs-induced terms, appearing in the form of a product of the primary shear strain and second harmonic normal strains in the equations. The corresponding 3rd SH waves components, which have not been spotted in the literature up to now, are thus named as the mixed 3rd SH waves, which will be further scrutinized in the following analyses.

Upon substituting the strain terms corresponding to the 1st SH wave field and 2nd Lamb wave field into Eqs. (9a) and (9b), the nonlinear stresses can be further expressed as

$$\sigma_{13}^{C} = A_{1}^{C}\left(\omega, y\right)\left(e^{i3k_{SH}^{L}x} - e^{i\left(\widetilde{k_{Lamb}^{Q}} + k_{SH}^{L}\right)x} \right) + A_{3}^{C}\left(\omega, y\right)e^{i3k_{SH}^{L}x} \tag{10a}$$

$$\sigma_{23}^{C} = A_{2}^{C}\left(\omega, y\right)\left(e^{i3k_{SH}^{L}x} - e^{i\left(\widetilde{k_{Lamb}^{Q}} + k_{SH}^{L}\right)x} \right) \tag{10b}$$

where $A_{1}^{C}\left(\omega, y\right)$ and $A_{2}^{C}\left(\omega, y\right)$ are related to TOECs and $A_{3}^{C}\left(\omega, y\right)$ to FOECs.

Then, by combining the reciprocity theory and the modal expansion method, Eq. (5a) can be again used to calculate the amplitude of the 3rd SH waves. Considering the nonlinear stresses in Eq. (10), the third harmonic amplitude takes the following form:

$$a_n^C(x) = A_4^C x e^{i3k_{SH}^L x} + A_5^C \left(e^{i\left(\widetilde{k_{Lamb}^Q} + k_{SH}^L\right)x} - e^{i\widetilde{k_{SH}^C} x} \right) + A_6^C x e^{i3k_{SH}^L x} \tag{11}$$

where A_4^C and A_5^C are related to TOECs and A_6^C to FOECs. Therefore, the first two terms represent the modal amplitude of the mixed 3rd SH waves. It can be seen that the first term exhibits a linearly cumulative amplitude with respect to the propagating distance while the second one shows a bounded amplitude. The combined effect of these two terms is a waveringly cumulative behavior of the mixed 3rd SH wave amplitude. On the contrary, the last term in Eq. (11) represents the pure 3rd SH waves whose amplitude is linearly cumulative.

To sum up, when the 1st SH waves propagate in a weakly nonlinear plate, the 3rd SH waves are generated through both TOECs and FOECs, as sketched in Fig. 2. The pure 3rd SH waves related to the FOECs are generated by the cubic self-interaction of the 1st SH waves. They are linearly cumulative due to their phase velocity matching with the 1st SH waves. By comparison, the mixed 3rd SH waves induced by the TOECs are generated through the quadratic mutual interaction between the 1st SH waves and their generated 2nd Lamb waves. Due to the mismatch of their phase velocities at most frequencies, the mixed 3rd SH waves show a waveringly cumulative character. Compared to the pure 3rd SH waves, the newly discovered mixed 3rd SH wave generation mechanism is less intuitive with unknown propagating characteristics up to now. Moreover, the

mixed 3rd SH waves may impact some SH-wave-based applications. For example, in those underwater inspection cases, the community shares the common belief that SH waves are immune to energy leakage into the surrounding liquid media, exemplified by the inspections of various underwater structures. The mixed 3rd harmonic SH waves, through the implication of the second Lamb waves in their generation, may challenge this belief and call for a meticulous reexamination of the problem. Another possible consequence is that the waveringly cumulative feature of the mixed 3rd SH waves may pose challenges to the cumulative-guided-wave-based damage detection methods which examine the slope of a line fitted from the nonlinear wave amplitude-wave propagating distance curve for damage characterization [11]. When using the 3rd SH waves, the waveringly cumulative feature may, in principle, affect the line fitting accuracy for damage detection. Therefore, this newly discovered mechanism deserves deeper analyses and validations, which will be addressed hereafter.

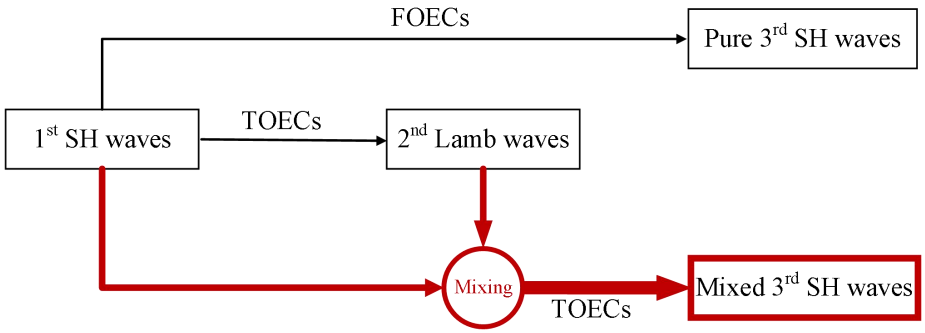

Figure 2. Mechanism of the third harmonic SH wave generation.

Numerical studies

Numerical studies are carried out to investigate the characteristics of the mixed 3rd SH waves, in

comparison with those of the pure 3rd SH waves. First, an FE model is briefly described with the justification on the FOECs of the material. After that, a complex-domain superposition method is proposed to extract the third harmonic responses. Finally, the properties of the mixed 3rd SH waves in terms of their influence and wave propagation characteristics are investigated.

Model description

An FE model is established in Abaqus/Explicit as shown in Fig. 3. An aluminum plate, 300 mm long and 2 mm thick, is investigated. Periodic boundary conditions are applied in the *z* direction so that plane waves can be simulated [19]. The excitation is a prescribed displacement in the *z* direction with an 8-cycle tone burst time-domain signal at 500 kHz. The amplitude of the displacement is set to 2 μm. Uniformly distributed displacement across the plate thickness is imposed to match the wave structure of the expectedly generated SH0 wave. The mesh size is set to 0.1 mm, which ensures more than 20 elements per smallest wavelength of interest as recommended in the literature [20, 21]. This results in a total of 240,000 elements and 945,315 degrees of freedom in the model. Convergence test has been conducted before subsequent analyses (not shown here). The material nonlinear elastic behaviors are introduced through the VUMAT module. The Landau TOECs of isotropic aluminum can be found in existing literature [22] while its Landau FOECs are not available to the best of our knowledge. Nevertheless, a related work provided FOECs of an aluminum crystal in terms of 11 Brugger constants [23]. Therefore, a conversion between the Brugger constants and Landau constants is conducted, through which the Landau FOECs for the isotropic aluminum are estimated. Details of the conversion and parameter estimation can be found in Appendix B. Although the obtained FOECs

may not be perfectly precise, they are believed to be in the realistic range. The material parameters used in the FE models are listed in Table 1.

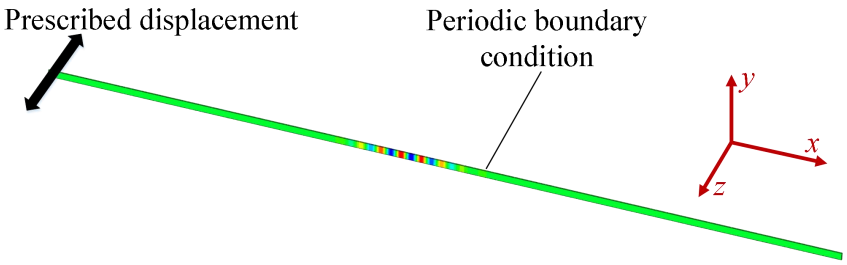

Figure 3. FE model description.

Table 1. Elastic constants of the aluminum plate in the FE model (Unit: GPa)

λ	μ	$\overline{A}$	$\overline{B}$	$\overline{C}$	$\overline{E}$	$\overline{F}$	$\overline{G}$	$\overline{H}$
55.27	25.95	-351.2	-140.4	-102.8	400	-406	347	72

Complex-domain Superposition method for signal separation and extraction

In order to characterize the third harmonic wave field, a complex-domain superposition method is proposed to extract the third harmonic responses in the time domain. The method takes the following steps:

1. Excite the plate with a tone burst signal $f(t)$ and get the system response which should contain both the linear and third harmonic components as

$$R_1 = g^L\left(f(t)\right) + g^C\left(\left(f(t)\right)^3\right) \tag{12}$$

2. Excite the plate again with the imaginary part of the previous excitation $if(t)$ which can be obtained with the Hilbert transform. The corresponding response can be expressed as

$$R_2 = g^L\left(if(t)\right) - ig^C\left(\left(if(t)\right)^3\right) = ig^L\left(f(t)\right) - ig^C\left(\left(f(t)\right)^3\right) \tag{13}$$

3. Multiply i to R_2 and superpose R_1 and iR_2. The linear responses can be eliminated and the third harmonic response can be obtained as

$$g^C\left(\left(f(t)\right)^3\right) = \frac{R_1 + iR_2}{2} \tag{14}$$

This procedure, named as the complex-domain superposition method, is analogous to the superposition method we proposed for the second harmonic extraction [24].

In order to validate the proposed method, a baseline method is used as the benchmark for which the nonlinear response is obtained by calculating the difference between the response of a system with material nonlinearity and that of its pure linear counterpart. It is worth noting that the difference signal contains both primary and third harmonic wave components since the third harmonic energy comes from the primary waves. A typical numerical example is examined for validation purposes. For the nonlinear system, only FOECs are involved. Displacement in the z direction for the SH waves is captured at 120 mm away from the excitation position. The overall response for the nonlinear system, dominated by the primary SH0 component, is shown in Fig. 4(a). The non-dispersive nature of the SH0 wave can be clearly observed as the number of cycles

of the received wave package is identical to that of the excitation. Then, the nonlinear response is calculated with both the baseline method and the complex-domain superposition method, with their comparisons shown in Fig. 4(b). After carrying out the fast Fourier Transform (FFT) on the windowed signals, the corresponding spectra are obtained and illustrated in Fig. 4(c). It can be seen that the third harmonic components obtained from the two methods match well. Moreover, the primary wave component is completely eliminated by the complex-domain superposition method, demonstrating the effectiveness of the proposed method in extracting and characterizing the third harmonic responses.

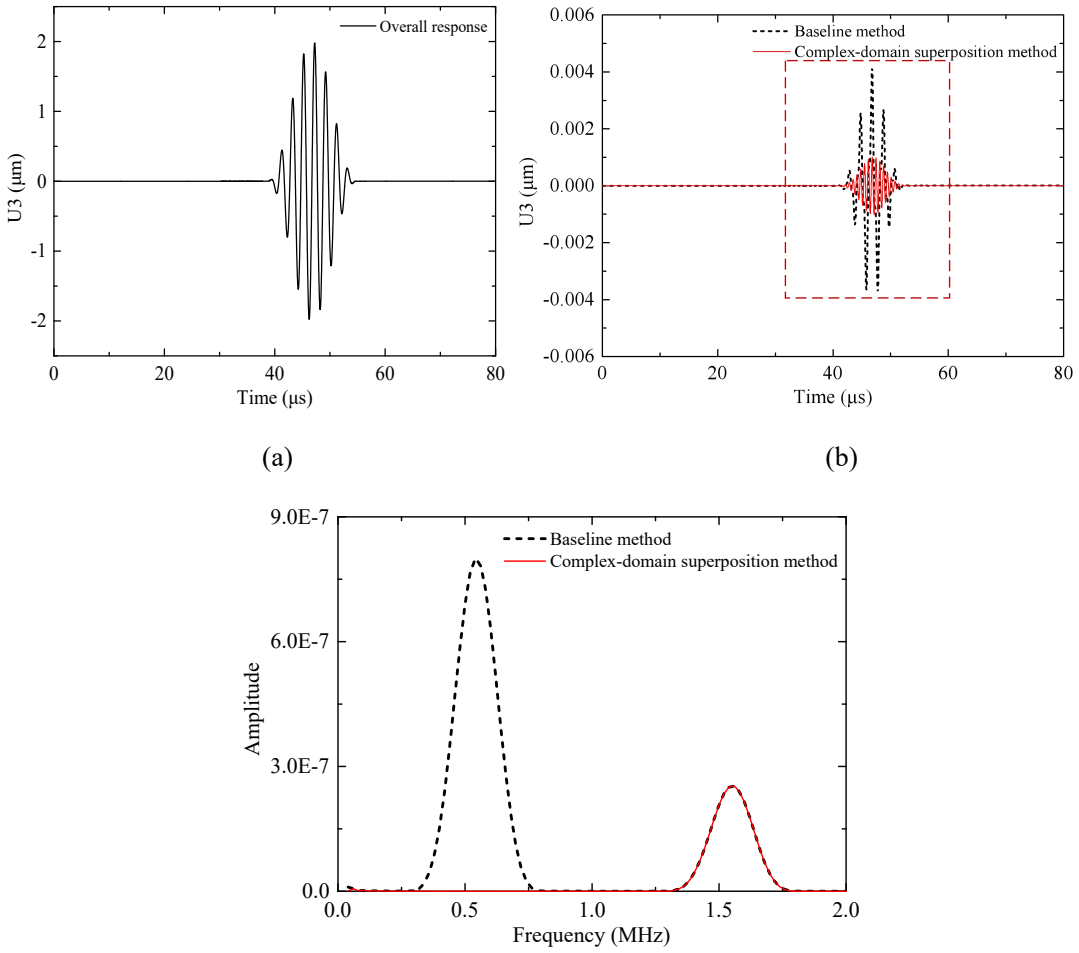

Figure 4. FE results for the validation of the third harmonic extraction method: (a) the overall

y-displacement response for the nonlinear system; (b) the third harmonic responses extracted with the baseline method and the proposed complex-domain superposition method; (c) the spectra of the third harmonic responses extracted with the two methods.

Characteristics of the mixed 3rd SH waves

With the proposed complex-domain superposition method, the influence of the GN, TOECs, and FOECs on the third harmonic generation is first evaluated. Through tactically introducing GN/TOECs/FOECs to the FE models, their corresponding third harmonic responses at 120 mm from the excitation position are extracted and compared in Fig. 5. It can be seen that the influence of GN is negligible compared with the other two cases associated with the material nonlinearity. This verifies the previous assumption of neglecting GN in the theoretical analyses. In addition, the third harmonic responses induced by TOECs and FOECs are in the same order of magnitude. This confirms the existence of both mixed and pure third harmonic SH waves and further indicates that the newly-discovered mixed third harmonic component is as important as the pure one in terms of energy level.

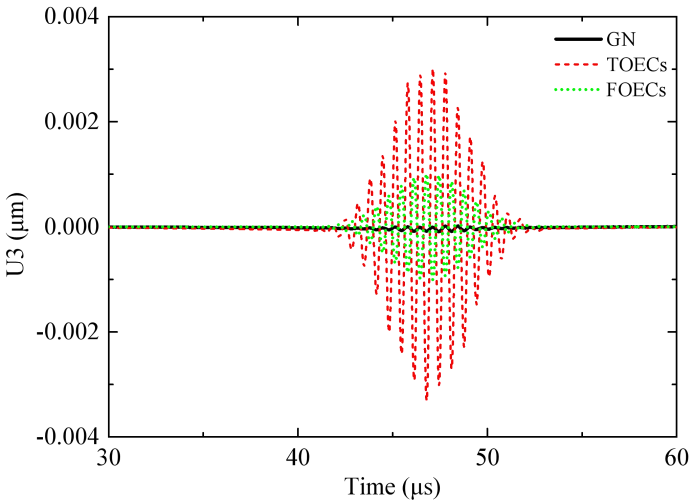

Figure 5. Influence of the GN, TOECs and FOECs on the third harmonic signals.

The propagating characteristics of the mixed 3rd SH waves are then investigated through comparisons with the pure ones. Note the theoretical analyses show the existence of a bounding term in the mixed 3rd SH waves (the second term on the right-hand-side of Eq. (11)). As an example, this term is calculated for the 500 kHz excitation case and its variation with respect to the propagating distance is plotted in Fig. 6. A bounding period is defined as the distance between the two dips as shown in Fig. 6. In this specific case, the bounding period is 9.1 mm.

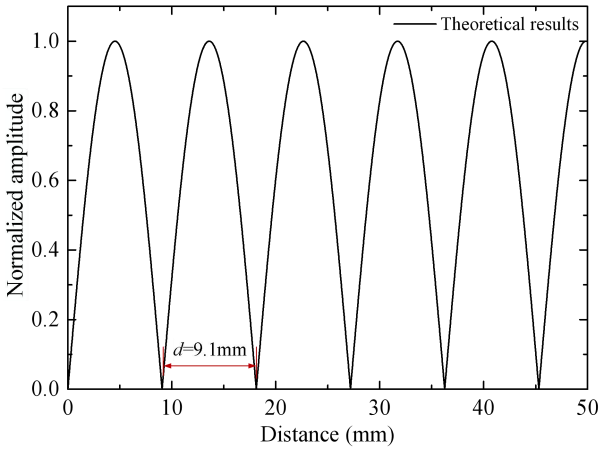

Figure 6. Characteristics of the theoretically calculated bounding term in the mixed 3rd SH waves.

In the FE simulations, the corresponding mixed and pure 3rd SH wave responses at different locations from 20 mm to 40 mm stepped by 2 mm, are calculated. As there are 11 time-domain third harmonic signals in each case, instead of presenting the time-domain signals, their amplitudes are extracted with the complex wavelet transform, detailed in our previous work [24], and plotted with respect to the wave propagating distance. Both the pure and mixed 3rd SH wave cases are studied with results compared in Fig. 7. It can be seen that the pure 3rd SH waves exhibit

a clear linearly cumulative characteristic (Fig. 7(a)) while the mixed 3rd SH waves are waveringly cumulative (Fig .7(b)) in amplitude with respect to the propagating distance. By further subtracting the fitted line from the third harmonic amplitudes from the FE simulations in Fig. 7(b), the difference is obtained in Fig. 8, showing a bounding behavior of the mixed 3rd SH wave amplitude, with a bounding period of around 9 mm, in agreement with the theoretical prediction in Fig. 6.

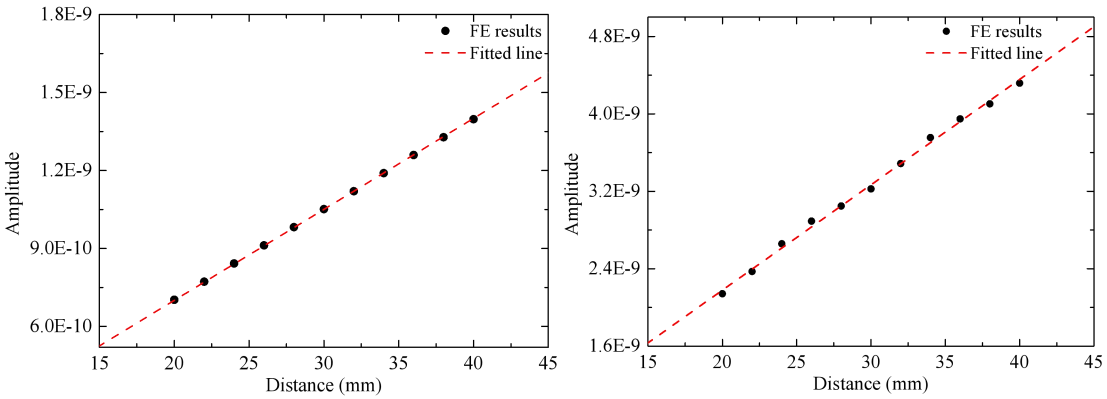

(a) (b)

Figure 7. Propagating characteristics of (a) pure and (b) mixed 3rd SH waves.

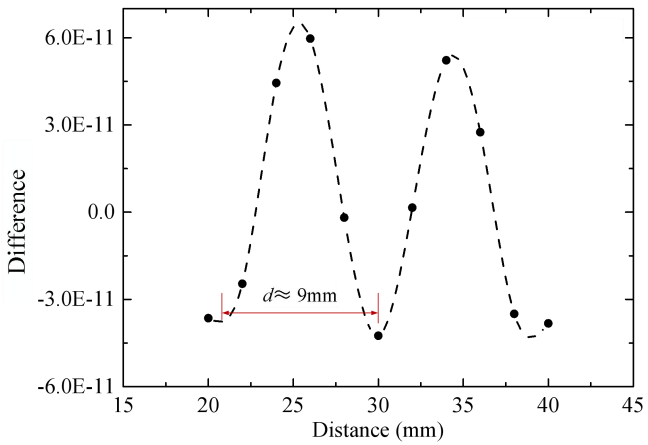

Figure 8. Bounding characteristics of the mixed 3rd SH waves from the FE results.

To sum up, FE studies confirm the existence of the mixed 3rd SH waves and establish the fact that they can be as important as the intuitive pure ones in terms of wave amplitude. Besides, the waveringly cumulative characteristic of the mixed 3rd SH waves is also well validated.

Experimental validations

Experiments are finally carried out to further ascertain the existence and the significance of the mixed 3rd SH waves. A direct scheme is first tested. After that, a specifically designed subtraction test scheme is proposed to mitigate the influence of undesired nonlinear sources in the measurement system.

Experimental design

Experiments are carried out on a 2 mm-thick aluminum (2024-T3) plate. Magnetostrictive Transducers (MsTs) are used for the SH wave excitation and reception with the dynamic magnetic field perpendicular to the static bias magnetic field. The spacing of the coil elements is 5.4 mm for the actuator and 1.8 mm for the receiver, which correspond to the half wavelengths of the 300 kHz and 900 kHz SH0 waves in an aluminum plate respectively. A RITEC RAM 5000 SNAP system is used to excite the MsT actuators with 100% output level. Meanwhile, 1024 signals captured by the MsT sensor are averaged and recorded by the oscilloscope.

The design of the experiments follows the following logic. In the experiments, both 3rd SH wave generation mechanism should affect the wave generation. Specifically, to identify the mixed

mechanism, a gel test is performed by placing a layer of gel on the SH wave propagating path. The gel allows an effective dissipation of the Lamb waves (out-of-plane particle motion) without, in principle, affecting the SH waves (in-plane particle motion) [25]. If the mixed 3rd harmonic SH waves (due to the mutual interaction between the 1st SH waves and their generated 2nd Lamb waves) do exist in the system, the overall third harmonic response of the system is expected to be changed by the presence of the gel. Otherwise, it should remain the same.

Direct test scheme

First, a direct test scheme is adopted with one pair of MsTs serving as the actuator and sensor respectively, as shown in Fig. 9. The plate, without gel, is excited with a 10-cycle tone burst signal at 300 kHz windowed by a Hann function and the received signal is shown in Fig. 10(a). Then, following the proposed complex-domain superposition method, the imaginary counterpart of the original excitation obtained with the Hilbert transform is applied to the actuator again. The third harmonic responses are further extracted, with the results displayed in Fig. 10(b). Through the FFT analysis on the windowed signals in both Figs. 10(a) and (b), their respective spectra are obtained and compared in Fig. 10(c). Results show that the third harmonic amplitude obtained with these two methods matches well. Again, this demonstrates the proposed complex-domain superposition method can effectively extract the third harmonic responses.

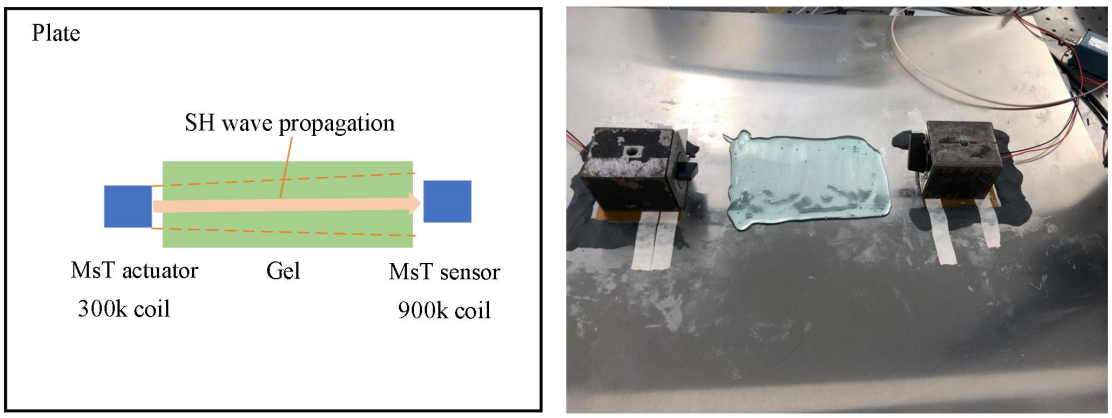

Figure 9. Direct scheme to validate the existence of the mixed 3rd SH waves.

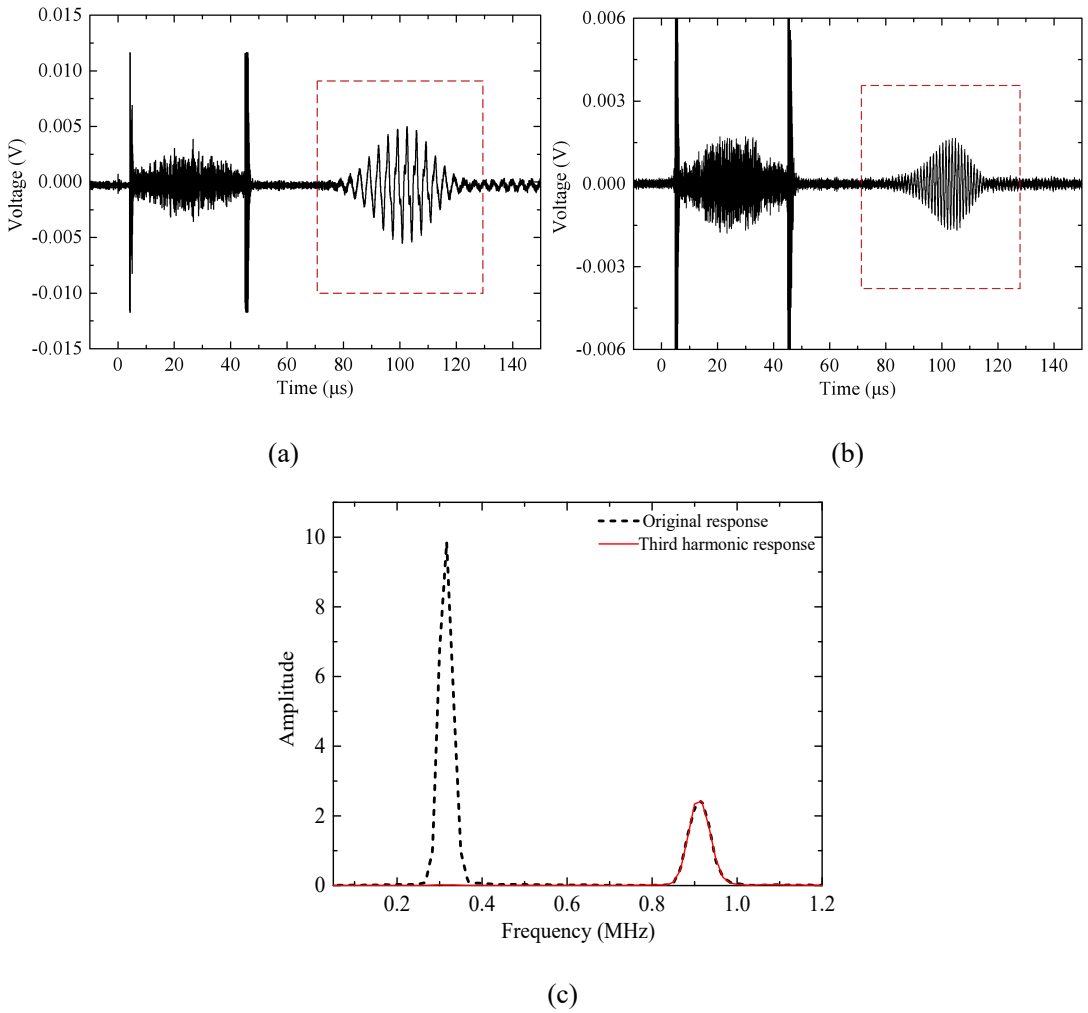

Figure 10. Signals captured in the system without gel on the plate: (a) overall response associated with the original excitation; (b) third harmonic response extracted with the complex-domain

superposition method; (c) spectra of the overall response and the extracted third harmonic response.

Upon the deployment of the gel on the plate, the third harmonic response is measured again following the same process and compared with the previous result without gel in Fig. 11. It can be seen that the third harmonic response remain almost the same after placing the gel. It is obvious that such a testing procedure fails to demonstrate the existence of the mixed 3rd SH waves. This is because the nonlinearity from the transducers and instruments overwhelms that of the aluminum plate, which will be addressed in the next section. Although the mixed third harmonic generation mechanism cannot be validated by this experimental scenario, results demonstrate two important points which are important to the further analyses. First, the signals received by the MsT are mainly the SH waves. Second, the gel indeed does not affect the SH wave field.

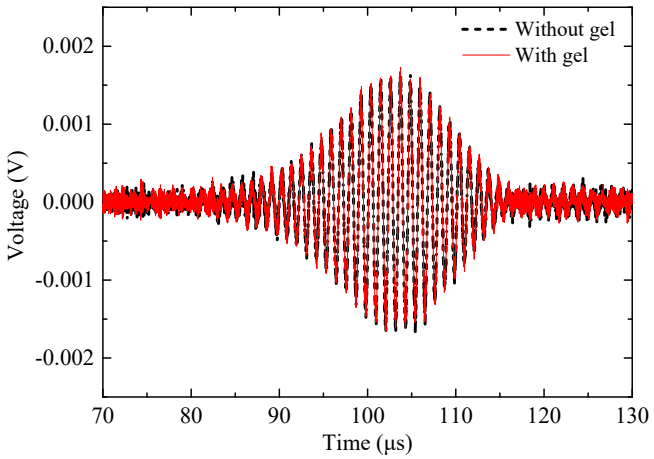

Figure 11. Comparison of the third harmonic responses before and after the placement of gel.

Subtraction test scheme

To mitigate the influence of the nonlinearities from the MsTs and the measurement system, a

subtraction test scheme is designed as illustrated in Fig. 12. The idea is inspired by Ref. [25] which addresses a counter-propagating SH wave mixing problem. Two MsT actuators are used to either simultaneously or independently generate SH waves in the plate through two independent channels of the RITEC RAM 5000 SNAP system. It is important to point out that although the angles of the MsT transducers are slightly twisted, the signals received will still be mainly associated with the SH waves. This is determined by the nature of the MsTs that only shear deformations can be generated or sensed when the dynamic magnetic field is perpendicular to the dynamic field in such devices [26, 27]. The subtraction test scheme is performed in two steps. First, both actuators 1 and 2 are simultaneously activated to excite SH waves at 300 kHz waves which mix in the plate. The corresponding received signal is denoted as T(1+2). Second, the two actuators are separately activated and the corresponding responses are marked as T(1) and T(2) respectively. The difference among these signals, T(1+2)-T(1)-T(2), referred to as the difference signal, is used for analyses. Since the third harmonic amplitude is proportional to the cubic of the primary wave amplitude and the primary SH waves generated by the two actuators superpose in the first test, the nonlinear responses induced by the material nonlinearity will remain in the difference signal. In addition, with the two actuators working separately, the influence of the nonlinearities at the actuating parts can be in principle minimized or eliminated in the difference signal. Therefore, this subtraction test scheme is expected to mitigate the undesired nonlinearities in the system.

Following the proposed procedure, experimental results for a plate without gel are shown in Fig. 13. The three original response signals are shown in Fig. 13(a). The difference signal is then

calculated and illustrated in Fig. 13(b), which is very weak and noisy. A Butterworth low-pass filter is then applied to the difference signal and the result is shown in Fig. 13(c), exhibiting a clear wave package. After taking the FFT to the windowed wave package in Fig. 13(c), the spectrum of the difference signal can be obtained, showing the wave components at the fundamental, second and third harmonics in Fig. 13(d). It is worth noting that the third harmonic amplitude, in this case, is two orders of magnitude smaller than that in Fig 10(c). This demonstrates that the nonlinearity of the measurement system was indeed significant in the previous direct tests, which is now effectively mitigated by the designed subtraction test scheme.

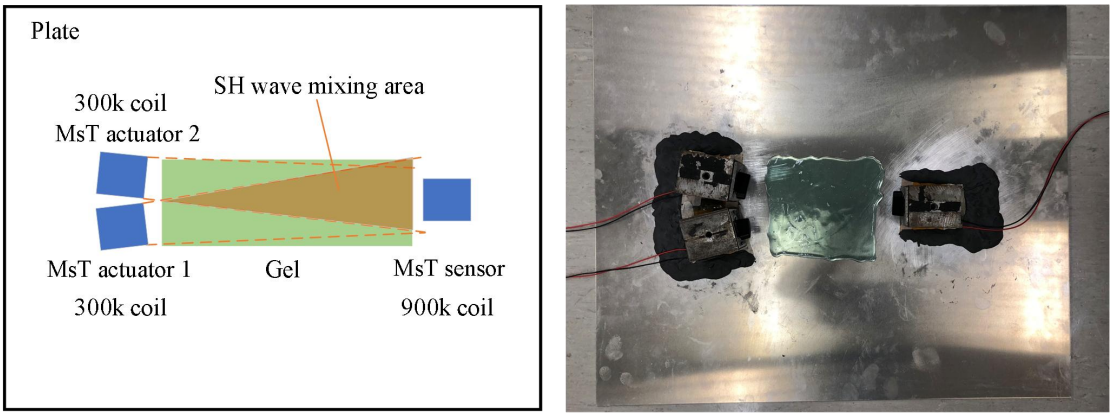

Figure 12. Subtraction scheme to validate the existence of the mixed third harmonic SH waves.

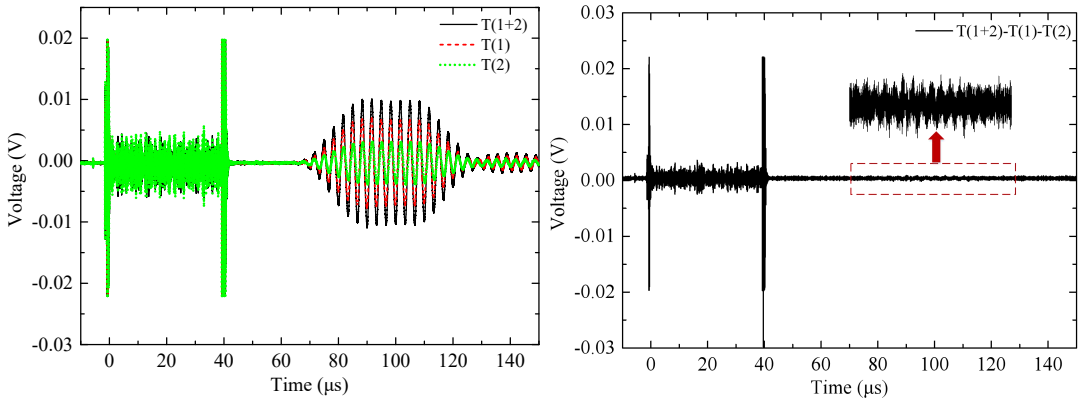

(a) (b)

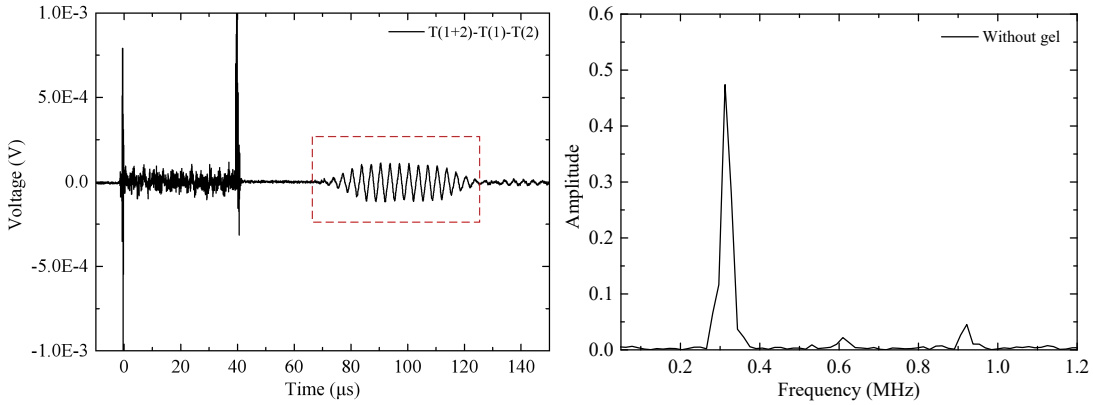

(c) (d)

Figure 13. Signals captured without gel on the plate: (a) responses when the actuators are simultaneously and separately activated; (b) difference signal; (c) filtered difference signal; (d) spectrum of the difference signal.

Then, the gel was placed on the wave propagating path as shown in Fig. 12 and the same test procedure is carried out to obtain the spectrum of the difference signal. Through comparing the results with and without gel in Fig. 14(a), two important observations can be highlighted. First, since the material-induced second harmonic SH waves cannot theoretically exist, the second harmonic component is attributed to the instrumentation nonlinearity. Second, focusing on the third harmonic response, a dramatic decrease in its amplitude can be observed with the deployment of the gel. After repeating the tests five times with corresponding error bars plotted in Fig. 14(b), the decreasing trend (around 30%) after the introduction of the gel is confirmed to be persistent. As the gel can only damp the Lamb waves, the experimentally observed decreasing trend of the third harmonic responses clearly demonstrates the existence of the mixed 3rd SH waves and its theoretically predicted generation mechanism, *e.g.* through the mutual interaction between the 1st SH waves and the 2nd Lamb waves. In addition, the approximately 30% decrease

proves its significance as a non-negligible 3rd SH wave component.

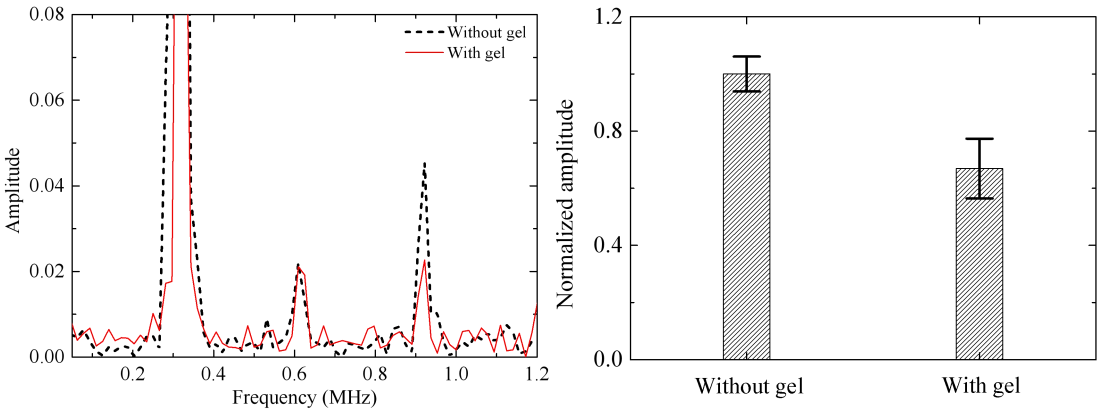

(a) (b)

Figure 14. Comparison of the third harmonic responses before and after the placement of gel: (a) spectra of the difference signals; (b) amplitude of the third harmonic components with error bars.

Conclusions

In this work, the mechanism of the third harmonic SH wave generation in a weakly nonlinear plate is investigated. In addition to the well-known pure third harmonic generation mechanism, a mixed mechanism is revealed. This newly discovered phenomenon, in terms of significance and propagating characteristics, is assessed and confirmed through finite element simulations and experiments. A complex-domain superposition method is proposed to extract the third harmonic wave components from the signals. For the identification of the mixed third harmonic SH waves, a gel test is proposed along with the establishment of a dedicated subtraction test scheme to mitigate undesired nonlinear sources in the measurement system.

Theoretical analyses show that, apart from the intuitive pure third harmonic generation caused by the cubic self-interaction of the 1st SH waves with FOECs, there exists another important path through which the so-called mixed third harmonic SH waves can be generated as a result of the quadratic mutual interaction between the 1st SH waves and their generated 2nd Lamb waves associated with only TOECs. The mixed 3rd SH waves exhibit waveringly cumulative feature at most frequencies where the phase velocities of the 1st SH waves and 2nd Lamb waves mismatch, in contrast to the linearly cumulative pure 3rd SH waves. The newly discovered mixed 3rd SH wave components can be as important as their conventional pure counterparts in terms of amplitude and energy level, which therefore are a non-negligible nonlinear factor to be considered in various applications.

The presented findings address the third harmonic generation mechanism at the fundamental level, paving the way for further explorations and applications of the 3rd SH-wave-based damage detection technology. Specifically, the newly discovered mixed third harmonic generation mechanism may impact on the further applications and call for a careful system design and a meticulous handling of the diagnosis signals, especially in the underwater cases considering the wave energy leakage or those cumulative-effect-based damage detection methods. This requires additional efforts to further explore the phenomena reported in this paper and assess their impact on future practical applications. In that sense, the developed finite element tools, the estimated FOECs and the proposed complex-domain superposition method can offer a convenient and comprehensive package for further investigations of the issue. Meanwhile, the proposed subtraction test scheme to mitigate the influence of the undesired nonlinear sources can be further

revamped and applied for engineering applications.

Acknowledgment

The project was supported by a grant from Research Grants Council of Hong Kong Special Administrative Region (PolyU 152070/16E). The authors would like to acknowledge Prof. Zhifeng Tang from Zhejiang University for providing us with the iron-cobalt foil made by his group.

Appendix A

The stress-strain relations for the nonlinear elastic material up to the third harmonics can be expressed as

$$\begin{aligned}\sigma_{11} &= \lambda(\varepsilon_{11}+\varepsilon_{22}+\varepsilon_{33})+2\mu\varepsilon_{11}+\overline{C}(\varepsilon_{11}+\varepsilon_{22}+\varepsilon_{33})^2+\overline{B}\left(\varepsilon_{11}^{\ 2}+\varepsilon_{22}^{\ 2}+\varepsilon_{33}^{\ 2}+2\varepsilon_{12}^{\ 2}+2\varepsilon_{13}^{\ 2}+2\varepsilon_{23}^{\ 2}\right)\\ &+2\overline{B}(\varepsilon_{11}+\varepsilon_{22}+\varepsilon_{33})\varepsilon_{11}+\overline{A}\left(\varepsilon_{11}^{\ 2}+\varepsilon_{12}^{\ 2}+\varepsilon_{13}^{\ 2}\right)+3\overline{E}(\varepsilon_{11}+\varepsilon_{22}+\varepsilon_{33})\left(\varepsilon_{11}^{\ 2}+\varepsilon_{12}^{\ 2}+\varepsilon_{13}^{\ 2}\right)\\ &+\overline{E}\left(\varepsilon_{11}^{\ 3}+\varepsilon_{22}^{\ 3}+\varepsilon_{33}^{\ 3}+3\varepsilon_{11}\varepsilon_{12}^{\ 2}+3\varepsilon_{11}\varepsilon_{13}^{\ 2}+3\varepsilon_{22}\varepsilon_{12}^{\ 2}+3\varepsilon_{33}\varepsilon_{13}^{\ 2}+3\varepsilon_{22}\varepsilon_{23}^{\ 2}+3\varepsilon_{33}\varepsilon_{23}^{\ 2}+6\varepsilon_{12}\varepsilon_{13}\varepsilon_{23}\right)\\ &+2\overline{F}(\varepsilon_{11}+\varepsilon_{22}+\varepsilon_{33})\left(\varepsilon_{11}^{\ 2}+\varepsilon_{22}^{\ 2}+\varepsilon_{33}^{\ 2}+2\varepsilon_{12}^{\ 2}+2\varepsilon_{13}^{\ 2}+2\varepsilon_{23}^{\ 2}\right)+2\overline{F}(\varepsilon_{11}+\varepsilon_{22}+\varepsilon_{33})^2\varepsilon_{11}\\ &+4\overline{G}\left(\varepsilon_{11}^{\ 2}+\varepsilon_{22}^{\ 2}+\varepsilon_{33}^{\ 2}+2\varepsilon_{12}^{\ 2}+2\varepsilon_{13}^{\ 2}+2\varepsilon_{23}^{\ 2}\right)\varepsilon_{11}+4\overline{H}(\varepsilon_{11}+\varepsilon_{22}+\varepsilon_{33})^3\end{aligned} \quad (A.1)$$

$$\begin{aligned}\sigma_{22} &= \lambda(\varepsilon_{11}+\varepsilon_{22}+\varepsilon_{33})+2\mu\varepsilon_{22}+\overline{C}(\varepsilon_{11}+\varepsilon_{22}+\varepsilon_{33})^{\ 2}+\overline{B}\left(\varepsilon_{11}^{\ 2}+\varepsilon_{22}^{\ 2}+\varepsilon_{33}^{\ 2}+2\varepsilon_{12}^{\ 2}+2\varepsilon_{13}^{\ 2}+2\varepsilon_{23}^{\ 2}\right)\\ &+2\overline{B}(\varepsilon_{11}+\varepsilon_{22}+\varepsilon_{33})\varepsilon_{22}+\overline{A}\left(\varepsilon_{21}^{\ 2}+\varepsilon_{22}^{\ 2}+\varepsilon_{23}^{\ 2}\right)+3\overline{E}(\varepsilon_{11}+\varepsilon_{22}+\varepsilon_{33})\left(\varepsilon_{12}^{\ 2}+\varepsilon_{22}^{\ 2}+\varepsilon_{23}^{\ 2}\right)\\ &+\overline{E}\left(\varepsilon_{11}^{\ 3}+\varepsilon_{22}^{\ 3}+\varepsilon_{33}^{\ 3}+3\varepsilon_{11}\varepsilon_{12}^{\ 2}+3\varepsilon_{11}\varepsilon_{13}^{\ 2}+3\varepsilon_{22}\varepsilon_{12}^{\ 2}+3\varepsilon_{3\ 3}\varepsilon_{13}^{\ 2}+3\varepsilon_{22}\varepsilon_{23}^{\ 2}+3\varepsilon_{33}\varepsilon_{23}^{\ 2}+6\varepsilon_{12}\varepsilon_{13}\varepsilon_{23}\right)\\ &+2\overline{F}(\varepsilon_{11}+\varepsilon_{22}+\varepsilon_{33})\left(\varepsilon_{11}^{\ 2}+\varepsilon_{22}^{\ 2}+\varepsilon_{33}^{\ 2}+2\varepsilon_{12}^{\ 2}+2\varepsilon_{13}^{\ 2}+2\varepsilon_{23}^{\ 2}\right)+2\overline{F}(\varepsilon_{11}+\varepsilon_{22}+\varepsilon_{33})^{\ 2}\varepsilon_{22}\\ &+4\overline{G}\left(\varepsilon_{11}^{\ 2}+\varepsilon_{22}^{\ 2}+\varepsilon_{33}^{\ 2}+2\varepsilon_{12}^{\ 2}+2\varepsilon_{13}^{\ 2}+2\varepsilon_{23}^{\ 2}\right)\varepsilon_{22}+4\overline{H}(\varepsilon_{11}+\varepsilon_{22}+\varepsilon_{33})^3\end{aligned} \quad (A.2)$$

$$\begin{aligned}\sigma_{33} &= \lambda(\varepsilon_{11}+\varepsilon_{22}+\varepsilon_{33})+2\mu\varepsilon_{33}+\overline{C}(\varepsilon_{11}+\varepsilon_{22}+\varepsilon_{33})^2+\overline{B}\left(\varepsilon_{11}{}^2+\varepsilon_{22}{}^2+\varepsilon_{33}{}^2+2\varepsilon_{12}{}^2+2\varepsilon_{13}{}^2+2\varepsilon_{23}{}^2\right)\\ &+2\overline{B}(\varepsilon_{11}+\varepsilon_{22}+\varepsilon_{33})\varepsilon_{33}+\overline{A}\left(\varepsilon_{33}{}^2+\varepsilon_{23}{}^2+\varepsilon_{13}{}^2\right)+3\overline{E}(\varepsilon_{11}+\varepsilon_{22}+\varepsilon_{33})\left(\varepsilon_{13}{}^2+\varepsilon_{23}{}^2+\varepsilon_{33}{}^2\right)\\ &+\overline{E}\left(\varepsilon_{11}{}^3+\varepsilon_{22}{}^3+\varepsilon_{33}{}^3+3\varepsilon_{11}\varepsilon_{12}{}^2+3\varepsilon_{11}\varepsilon_{13}{}^2+3\varepsilon_{22}\varepsilon_{12}{}^2+3\varepsilon_{33}\varepsilon_{13}{}^2+3\varepsilon_{22}\varepsilon_{23}{}^2+3\varepsilon_{33}\varepsilon_{23}{}^2+6\varepsilon_{12}\varepsilon_{13}\varepsilon_{23}\right)\\ &+2\overline{F}(\varepsilon_{11}+\varepsilon_{22}+\varepsilon_{33})\left(\varepsilon_{11}{}^2+\varepsilon_{22}{}^2+\varepsilon_{33}{}^2+2\varepsilon_{12}{}^2+2\varepsilon_{13}{}^2+2\varepsilon_{23}{}^2\right)+2\overline{F}(\varepsilon_{11}+\varepsilon_{22}+\varepsilon_{33})^2\varepsilon_{33}\\ &+4\overline{G}\left(\varepsilon_{11}{}^2+\varepsilon_{22}{}^2+\varepsilon_{33}{}^2+2\varepsilon_{12}{}^2+2\varepsilon_{13}{}^2+2\varepsilon_{23}{}^2\right)\varepsilon_{33}+4\overline{H}(\varepsilon_{11}+\varepsilon_{22}+\varepsilon_{33})^3\end{aligned} \tag{A.3}$$

$$\begin{aligned}\sigma_{12} &= 2\mu\varepsilon_{12}+2\overline{B}(\varepsilon_{11}+\varepsilon_{22}+\varepsilon_{33})\varepsilon_{12}+\overline{A}\left(\varepsilon_{11}\varepsilon_{12}+\varepsilon_{22}\varepsilon_{12}+\varepsilon_{31}\varepsilon_{32}\right)+2\overline{F}(\varepsilon_{11}+\varepsilon_{22}+\varepsilon_{33})^2\varepsilon_{12}\\ &+3\overline{E}(\varepsilon_{11}+\varepsilon_{22}+\varepsilon_{33})\left(\varepsilon_{11}\varepsilon_{12}+\varepsilon_{22}\varepsilon_{12}+\varepsilon_{31}\varepsilon_{32}\right)+4\overline{G}\left(\varepsilon_{11}{}^2+\varepsilon_{22}{}^2+\varepsilon_{33}{}^2+2\varepsilon_{12}{}^2+2\varepsilon_{13}{}^2+2\varepsilon_{23}{}^2\right)\varepsilon_{12}\end{aligned} \tag{A.4}$$

$$\begin{aligned}\sigma_{13} &= 2\mu\varepsilon_{13}+2\overline{B}(\varepsilon_{11}+\varepsilon_{22}+\varepsilon_{33})\varepsilon_{13}+\overline{A}\left(\varepsilon_{11}\varepsilon_{13}+\varepsilon_{33}\varepsilon_{31}+\varepsilon_{32}\varepsilon_{21}\right)+2\overline{F}(\varepsilon_{11}+\varepsilon_{22}+\varepsilon_{33})^2\varepsilon_{13}\\ &+3\overline{E}(\varepsilon_{11}+\varepsilon_{22}+\varepsilon_{33})\left(\varepsilon_{11}\varepsilon_{13}+\varepsilon_{33}\varepsilon_{13}+\varepsilon_{12}\varepsilon_{32}\right)+4\overline{G}\left(\varepsilon_{11}{}^2+\varepsilon_{22}{}^2+\varepsilon_{33}{}^2+2\varepsilon_{12}{}^2+2\varepsilon_{13}{}^2+2\varepsilon_{23}{}^2\right)\varepsilon_{13}\end{aligned} \tag{A.5}$$

$$\begin{aligned}\sigma_{23} &= 2\mu\varepsilon_{23}+2\overline{B}(\varepsilon_{11}+\varepsilon_{22}+\varepsilon_{33})\varepsilon_{23}+\overline{A}\left(\varepsilon_{23}\varepsilon_{33}+\varepsilon_{22}\varepsilon_{23}+\varepsilon_{13}\varepsilon_{21}\right)+2\overline{F}(\varepsilon_{11}+\varepsilon_{22}+\varepsilon_{33})^2\varepsilon_{23}\\ &+3\overline{E}(\varepsilon_{11}+\varepsilon_{22}+\varepsilon_{33})\left(\varepsilon_{22}\varepsilon_{23}+\varepsilon_{33}\varepsilon_{23}+\varepsilon_{12}\varepsilon_{13}\right)+4\overline{G}\left(\varepsilon_{11}{}^2+\varepsilon_{22}{}^2+\varepsilon_{33}{}^2+2\varepsilon_{12}{}^2+2\varepsilon_{13}{}^2+2\varepsilon_{23}{}^2\right)\varepsilon_{23}\end{aligned} \tag{A.6}$$

Appendix B

Denote the Lagrangian strain tensor as

$$\mathbf{E}=\begin{bmatrix} E_1 & \frac{1}{2}E_6 & \frac{1}{2}E_5 \\ \frac{1}{2}E_6 & E_2 & \frac{1}{2}E_4 \\ \frac{1}{2}E_5 & \frac{1}{2}E_4 & E_3 \end{bmatrix} \tag{B.1}$$

The strain energy of the an isotropic material can be expressed with the Brugger's model [23, 28], as

$$W=\psi_2+\psi_3+\psi_4 \tag{B.2}$$

$$\psi_2=\frac{1}{2}c_{11}\left(E_1{}^2+E_2{}^2+E_3{}^2\right)+c_{12}\left(E_1E_2+E_2E_3+E_3E_1\right)+\frac{1}{2}c_{44}\left(E_4{}^2+E_5{}^2+E_6{}^2\right) \tag{B.3}$$

$$\begin{aligned}\psi_3 = &\frac{1}{6}c_{111}\left(E_1^{\,3}+E_2^{\,3}+E_3^{\,3}\right)+\frac{1}{2}c_{112}\left(E_2E_1^{\,2}+E_3E_1^{\,2}+E_1E_2^{\,2}+E_3E_2^{\,2}+E_1E_3^{\,2}+E_2E_3^{\,2}\right)\\ &+c_{123}E_1E_2E_3+\frac{1}{2}c_{144}\left(E_1E_4^{\,2}+E_2E_5^{\,2}+E_3E_6^{\,2}\right)\\ &+\frac{1}{2}c_{155}\left(E_2E_4^{\,2}+E_3E_4^{\,2}+E_1E_5^{\,2}+E_3E_5^{\,2}+E_1E_6^{\,2}+E_2E_6^{\,2}\right)+c_{456}E_4E_5E_6\end{aligned} \tag{B.4}$$

$$\begin{aligned}\psi_4 = &\frac{1}{24}c_{1111}\left(E_1^{\,4}+E_2^{\,4}+E_3^{\,4}\right)+\frac{1}{6}c_{1112}\left[E_1^{\,3}\left(E_2+E_3\right)+E_2^{\,3}\left(E_1+E_3\right)+E_3^{\,3}\left(E_1+E_2\right)\right]\\ &+\frac{1}{4}c_{1122}\left(E_1^{\,2}E_2^{\,2}+E_2^{\,2}E_3^{\,2}+E_3^{\,2}E_1^{\,2}\right)+\frac{1}{2}c_{1123}\left(E_1^{\,2}E_2E_3+E_2^{\,2}E_1E_3+E_3^{\,2}E_1E_2\right)\\ &+\frac{1}{4}c_{1144}\left(E_1^{\,2}E_4^{\,2}+E_2^{\,2}E_5^{\,2}+E_3^{\,2}E_6^{\,2}\right)+\frac{1}{4}c_{1155}\left[E_1^{\,3}\left(E_5+E_6\right)+E_2^{\,3}\left(E_4+E_6\right)+E_3^{\,3}\left(E_4+E_5\right)\right]\\ &+\frac{1}{2}c_{1255}\left[E_1E_2\left(E_4^{\,2}+E_5^{\,2}\right)+E_2E_3\left(E_6^{\,2}+E_5^{\,2}\right)+E_1E_3\left(E_4^{\,2}+E_6^{\,2}\right)\right]\\ &+\frac{1}{2}c_{1266}\left(E_1E_2E_6^{\,2}+E_2E_3E_4^{\,2}+E_1E_3E_5^{\,2}\right)+c_{1456}\left[E_4E_5E_6\left(E_1+E_2+E_3\right)\right]\\ &+\frac{1}{24}c_{4444}\left(E_4^{\,4}+E_5^{\,4}+E_6^{\,4}\right)+\frac{1}{4}c_{4455}\left(E_4^{\,2}E_5^{\,2}+E_5^{\,2}E_6^{\,2}+E_4^{\,2}E_6^{\,2}\right)\end{aligned} \tag{B.5}$$

where c_{ij}, c_{ijk} and the c_{ijkl} are the Brugger second, third and fourth order constants. Meanwhile, the strain energy can be also expressed with the Murnaghan constants [2, 29], as

$$W=\frac{\lambda+2\mu}{2}i_1^{\,2}-2\mu i_2+\frac{l+2m}{3}i_1^{\,3}-mi_1i_2+ni_3+p_1i_1^{\,4}+p_2i_1^{\,2}i_2+p_3i_1i_3+p_4i_2^{\,2} \tag{B.6}$$

$$i_1=\mathrm{tr}(\mathbf{E}),\quad i_2=\frac{1}{2}\left[\left(\mathrm{tr}(\mathbf{E})\right)^2-\mathrm{tr}(\mathbf{E}^2)\right],\quad i_3=\det(\mathbf{E}) \tag{B.7}$$

where l,m,n and p_1, p_2, p_3, p_4 are the Murnaghan third and fourth order constants. det() denotes the determinant. Through comparisons between the coefficients, the relationship between the Brugger constants and Murnaghan constants can be established as,

$$
\begin{aligned}
c_{11}&=\lambda+2\mu\\
c_{12}&=\lambda\text{-}2\mu\\
c_{44}&=2\mu
\end{aligned}
\qquad
\begin{aligned}
c_{111}&=2l+4m\\
c_{112}&=2l\\
c_{123}&=2l-2m+n\\
c_{144}&=m-\frac{n}{2}\\
c_{155}&=m\\
c_{456}&=\frac{n}{4}
\end{aligned}
\qquad
\begin{aligned}
c_{1111}&=24p_1\\
c_{1112}&=24p_1+12p_2\\
c_{1122}&=24p_1+16p_2+16p_4\\
c_{1123}&=24p_1+20p_2+2p_3+16p_4\\
c_{1144}&=-2p_2-12p_3\\
c_{1155}&=-2p_2\\
c_{1255}&=-2p_2-\frac{p_3}{2}-4p_4\\
c_{1266}&=-2p_2-4p_4\\
c_{1456}&=\frac{p_3}{4}\\
c_{4444}&=6p_4\\
c_{4455}&=2p_4
\end{aligned}
\tag{B.8}
$$

For isotropic materials, there should be only two independent SOECs, three independent TOECs and four independent FOECs. Therefore, the inherent relations among the Brugger constants for isotropic materials can be further calculated from Eq. (B8), as

$$
c_{44}=\frac{c_{11}\text{-}c_{12}}{2}
\qquad
\begin{aligned}
c_{111}&=c_{123}+6c_{144}+8c_{456}\\
c_{112}&=c_{123}+2c_{144}\\
c_{155}&=c_{144}+2c_{456}
\end{aligned}
\qquad
\begin{aligned}
c_{1112}&=c_{1111}-6c_{1155}\\
c_{1122}&=c_{1111}-8c_{1155}+\frac{8}{3}c_{4444}\\
c_{1123}&=c_{1111}-10c_{1155}+8c_{1456}+\frac{8}{3}c_{4444}\\
c_{1144}&=c_{1155}-4c_{1456}\\
c_{1255}&=c_{1155}-2c_{1456}-\frac{2}{3}c_{4444}\\
c_{1266}&=c_{1155}-\frac{2}{3}c_{4444}\\
c_{4455}&=\frac{1}{3}c_{4444}
\end{aligned}
\tag{B.9}
$$

The obtained relationship among the Brugger constants agrees with the ones provided in [26], demonstrating the correctness of the derivation.

From the existing Brugger FOECs for aluminum crystals, 11 constants are given in Ref. [23]. We take four to be the independent ones (c_{1111}=9916 GPa , c_{1155}=3554 GPa , c_{1122}=3708 GPa , $c_{1123}=-1000$ GPa) and use them to estimate the Murnaghan FOECs for isotropic aluminum material. Finally, as the Landau-Lifshitz model is used in the paper, the Landau FOECs can be calculated from the relationship between the Murnaghan FOECs and Landau FOECs provided in Ref. [29], as

$$\begin{aligned} p_1 &= \overline{E} + \overline{F} + \overline{G} + \overline{H} \\ p_2 &= -3\overline{E} - 2\overline{F} - 4\overline{G} \\ p_3 &= 3\overline{E} \\ p_4 &= 4\overline{G} \end{aligned} \tag{B.10}$$

References

[1] Jhang K Y.Nonlinear ultrasonic techniques for nondestructive assessment of micro damage in material: a review. International journal of precision engineering and manufacturing, **10** (1): 123-135, 2009.

[2] Chillara V K and C J Lissenden.Review of nonlinear ultrasonic guided wave nondestructive evaluation: theory, numerics, and experiments. Optical Engineering, **55** (1): 011002, 2015.

[3] Müller M F, J Y Kim, J Qu and L J Jacobs.Characteristics of second harmonic generation of Lamb waves in nonlinear elastic plates. The Journal of the Acoustical Society of America, **127** (4): 2141-2152, 2010.

[4] Deng M.Analysis of second-harmonic generation of Lamb modes using a modal analysis approach. Journal of applied physics, **94** (6): 4152-4159, 2003.

[5] De Lima W and M Hamilton.Finite-amplitude waves in isotropic elastic plates. Journal of sound and vibration, **265** (4): 819-839, 2003.

[6] Liu Y, V K Chillara and C J Lissenden.On selection of primary modes for generation of strong internally resonant second harmonics in plate. Journal of Sound and Vibration, **332** (19): 4517-4528, 2013.

[7] Pruell C, J-Y Kim, J Qu and L J Jacobs.Evaluation of plasticity driven material damage using Lamb waves. Applied Physics Letters, **91** (23): 231911, 2007.

[8] Deng M and J Pei.Assessment of accumulated fatigue damage in solid plates using nonlinear Lamb wave approach. Applied physics letters, **90** (12): 121902, 2007.

[9] Xiang Y, M Deng, F Z Xuan and C J Liu.Experimental study of thermal degradation in ferritic Cr–Ni alloy steel plates using nonlinear Lamb waves. Ndt & E International, **44** (8): 768-774, 2011.

[10] Rauter N and R Lammering.Numerical simulation of elastic wave propagation in isotropic media considering material and geometrical nonlinearities. Smart Materials and Structures, **24** (4): 045027, 2015.

[11] Wan X, P Tse, G Xu, T Tao and Q Zhang.Analytical and numerical studies of approximate phase velocity matching based nonlinear S0 mode Lamb waves for the detection of evenly distributed microstructural changes. Smart Materials and Structures, **25** (4): 045023, 2016.

[12] Liu Y, V K Chillara, C J Lissenden and J L Rose.Third harmonic shear horizontal and Rayleigh Lamb waves in weakly nonlinear plates. Journal of Applied Physics, **114** (11): 114908, 2013.

[13] Lissenden C, Y Liu, G Choi and X Yao.Effect of localized microstructure evolution on higher harmonic generation of guided waves. Journal of Nondestructive Evaluation, **33** (2): 178-186, 2014.

[14] Liu Y, C J Lissenden and J L Rose. Microstructural characterization in plates using guided wave third harmonic generation. AIP Conference Proceedings, 1581(1): 639-645, 2014.

[15] Mu X, X Gu, M V Makarov, Y J Ding, J Wang, J Wei and Y Liu.Third-harmonic generation by cascading second-order nonlinear processes in a cerium-doped KTiOPO 4 crystal. Optics letters, **25** (2): 117-119, 2000.

[16] Liu Y. 2014. Characterization of global and localized material degradation in plates and cylinders via nonlinear interaction of ultrasonic guided waves. *Dissertation*, The Pennsylvania State University.

[17] Giurgiutiu V, *Structural health monitoring: with piezoelectric wafer active sensors*. (Elsevier, 2007).

[18] Santoni G. 2010. Fundamental studies in the Lamb-wave interaction between piezoelectric wafer active sensor and host structure during structural health monitoring. *Dissertation*, University of South Carolina.

[19] Wu W, J Owino, A Al-Ostaz, et al. Applying periodic boundary conditions in finite element analysis. SIMULIA Community Conference, Providence, 2014.

[20] Moser F, L J Jacobs and J Qu. Modeling elastic wave propagation in waveguides with the finite element method. Ndt & E International, **32**(4): 225-234, 1999.

[21] Willberg C, S Duczek, J M V Perez, et al. Comparison of different higher order finite element schemes for the simulation of Lamb waves. Computer Methods in Applied Mechanics and Engineering, **241**: 246-261, 2012.

[22] Choi G, Liu Y, Lissenden C J, et al. Influence of localized microstructure evolution on second harmonic generation of guided waves. AIP Conference Proceedings. AIP, 1581(1): 631-638, 2014.

[23] Wang H and M Li.Ab initio calculations of second-, third-, and fourth-order elastic constants for single crystals. Physical Review B, **79** (22): 224102, 2009.

[24] Shan S, L Cheng and P Li.Adhesive nonlinearity in Lamb-wave-based structural health monitoring systems. Smart Materials and Structures, **26** (2): 025019, 2016.

[25] Hasanian M and C J Lissenden.Second order harmonic guided wave mutual interactions in plate: Vector analysis, numerical simulation, and experimental results. Journal of Applied

Physics, **122** (8): 084901, 2017.

[26] Kim Y Y and Y E Kwon.Review of magnetostrictive patch transducers and applications in ultrasonic nondestructive testing of waveguides. Ultrasonics, **62** 3-19, 2015.

[27] Lee J S, Y Y Kim and S H Cho.Beam-focused shear-horizontal wave generation in a plate by a circular magnetostrictive patch transducer employing a planar solenoid array. Smart Materials and Structures, **18** (1): 015009, 2008.

[28] Landolt H, K Hellwege, R Börnstein and O Madelung, *Landolt-Bornstein Numerical Data and Functional Relationships in Science and Technology: New Series. Crystal and Solid State Physics. Group III.* (Springer-Verlag, 1966).

[29] Destrade M and R W Ogden.On the third-and fourth-order constants of incompressible isotropic elasticity. The Journal of the Acoustical Society of America, **128** (6): 3334-3343, 2010.